



Osteoblastic and anti-osteoclastic activities of strontium-substituted silicocarnotite ceramics: *In vitro* and *in vivo* studies

Junkai Zeng^{a,1}, Jingshu Guo^{b,1}, Zhenyu Sun^a, Fanyan Deng^b, Congqin Ning^{b,**}, Youzhan Xie^{a,*}

^a Shanghai Key Laboratory of Orthopaedic Implants, Department of Orthopaedic Surgery, Shanghai Ninth People's Hospital, Shanghai Jiaotong University School of Medicine, Shanghai, China

^b State Key Laboratory of High Performance Ceramics and Superfine Microstructure, Shanghai Institute of Ceramics, Chinese Academy of Sciences, Shanghai, 200050, China

ARTICLE INFO

Keywords:

Strontium
Bioceramics
Osteoblastic
Osteoclastic
Silicocarnotite

ABSTRACT

Osteoporosis bone defect is a refractory orthopaedic disease which characterized by impaired bone quality and bone regeneration capacity. Current therapies, including antiosteoporosis drugs and artificial bone grafts, are not always satisfactory. Herein, a strontium-substituted calcium phosphate silicate bioactive ceramic (Sr-CPS) was fabricated. In the present study, the extracts of Sr-CPS were prepared for *in vitro* study and Sr-CPS scaffolds were used for *in vivo* study. The cytocompatibility, osteogenic and osteoclastogenic properties of Sr-CPS extracts were characterized in comparison to CPS. Molecular mechanisms were also evaluated by Western blot. Sr-CPS extracts were found to promote osteogenesis by upregulating Wnt/ β -catenin signal pathways and inhibit osteoclastogenesis through downregulating NF- κ B signal pathway. *In vivo*, micro-CT, histological and histomorphometric observation were conducted after 8 weeks of implantation to evaluate the bone formation using calvarial defects model in ovariectomized rats. Compared with CPS, Sr-CPS significantly promoted critical sized ovariectomy (OVX) calvarial defects healing. Among all the samples, Sr-10 showed the best performance due to a perfect match of bone formation and scaffold degradation rates. Overall, the present study demonstrated that Sr-CPS ceramic can dually modulate both bone formation and resorption, which might be a promising candidate for the reconstruction of osteoporotic bone defect.

1. Introduction

Osteoporosis, which commonly happened in elderly people, is characterized by low bone mineral density (BMD), degeneration of bone microstructure and increased bone fragility [1]. Osteoporosis is closely related to the decrease in bone quality, which further leads to an increased risk in fragility fractures and bone defect. These complications result in lower life quality, higher mortality and health-care costs [2]. Additionally, it is estimated that more than 450 million people in the world will be over 65 years of age in the next 20 years [3]. With an ageing population, the prevalence of osteoporosis, especially postmenopausal osteoporosis, will be further expanded and its medical and socioeconomic effects have drawn great attentions.

Compared with usual fractures, the treatment of osteoporotic fractures is more complicated. Firstly, the patient population is characterized by advanced age and usually accompanied by impaired physical

and immune function, resulting in poor compensatory function and longer recovery process [4]. Secondly, osteoporosis has a negative impact on healing capacity of bone because of weakened osteoblast activity and hyperfunctioning of osteoclasts [5]. When bone resorption predominates over bone formation, endochondral bone formation is inhibited and the mechanical property of the fractured callus is impaired, leading to a delayed healing of fractures or defects [6]. Thirdly, impaired bone quality often leads to comminution at the fracture site, and the difficulty of reduction and fixation is further increased during the surgery [7]. Long period of bed rest not only costs a lot of time and money, but also leads to rapid bone loss, and then generates a vicious circle, which results in re-fracture, seriously damaging the life quality of patients and even causing disability and death [8]. Therefore, the treatment of osteoporotic fracture is still a challenging task in orthopaedics.

Bone grafting materials are usually necessary for repairing

Peer review under responsibility of KeAi Communications Co., Ltd.

* Corresponding author.

** Corresponding author.

E-mail addresses: cqning@mail.sic.ac.cn (C. Ning), drxie_miss@163.com (Y. Xie).

¹ These authors contributed equally to this work.

<https://doi.org/10.1016/j.bioactmat.2020.03.008>

Received 10 February 2020; Received in revised form 17 March 2020; Accepted 18 March 2020

2452-199X/© 2020 Production and hosting by Elsevier B.V. on behalf of KeAi Communications Co., Ltd. This is an open access article under the CC BY-NC-ND license (<http://creativecommons.org/licenses/by-nc-nd/4.0/>).

osteoporotic bone defects. Autologous bone is still considered the clinical “gold standard” and the most effective method for bone regeneration [9]. Autograft could significantly induce direct bone bonding and stem cells osteogenic differentiation without any immune response [10]. However, there are unavoidable complications for patients after auto-transplantation, such as excessive pain and blood loss, destruction of normal structure at the donor site, risk of bacterial infection, etc. Additionally, due to the limitation of natural bone supply, artificial bone substitutes are increasingly being used in the treatment of bone defects to overcome the disadvantages of using autologous or allogenic bone grafts.

Calcium phosphate ceramics (CaP), one of the most popular implantable materials, have been widely used in orthopaedics due to their excellent biocompatibility [11]. However, their bioactivity and osteogenic capacity are limited [12]. The above drawbacks have limited its application in segmental bone defect. Silicon (Si) is a vital trace element for bone development and silicon-based biomaterials have been proved to possess great bioactivity [13,14]. To combine the advantages of calcium phosphate ceramics and silicon element, we synthesized silicon-containing calcium phosphates ceramics with a silicocarnotite structure ($\text{Ca}_5(\text{PO}_4)_2\text{SiO}_4$, CPS) by a sol-gel method in the previous study [15]. As a promising material for bone regeneration applications, CPS showed a superior cytocompatibility and promoted the osteogenic differentiation of rat bone marrow-derived mesenchymal stem cells (rBMSC) [11].

For osteoporotic fractures and bone defects, antiosteoporosis drugs are usually administered as an adjunctive therapy for surgery to promote new bone formation and reduce the risk of re-fractures. At present, antiosteoporosis drugs mainly include selective estrogen receptor modulators (SERMs), estrogen, bisphosphonates, calcitonin, etc [16]. The main role of the antiosteoporosis drugs is to regulate hyperactive bone resorption. However, they are arduous to reach the defect area and promote local bone regeneration. Clinically, bioinert materials such as metal and polymethylmethacrylate (PMMA) were commonly used as internal fixation. But they lack bioactivity and only serve as temporary fixation to provide temporary mechanical support. Regulating osteoblast and osteoclast activity at the defect site by bioactive materials is a new idea to accelerate osteoporosis bone defect healing.

Strontium (Sr) is an alkaline earth metal, which normally exists in the human bone [17]. Sr^{2+} ions can enhance the density of the bone tissue via improving osteoblast activity and inhibiting osteoclast function [18]. Furthermore, Sr^{2+} has been widely applied in the osteoporosis therapy since 1950's and oral administration is the most common way [19]. However, the bioavailability of the Sr^{2+} is only about 25% by oral medication [20]. For osteoporosis bone defect, local administration of Sr^{2+} with a bioactive implant is more efficient.

Yang et al. found that Sr activates the Wnt/ β -catenin signaling pathway to promote the *in vitro* differentiation of MSCs and *in vivo* bone formation [21]. Other studies have showed that Sr suppresses osteoclastogenesis by disturbing the NF- κ B pathway [22]. Sr is a homologous element of Ca, it is assumed that small amount addition of Sr into CPS could form a Sr substituted solid solution, which is expected to have synergetic effects during bone healing, i.e. dual biological functions of promoting osteogenesis and anti-osteoclastogenesis. In the present study, Sr-doped calcium phosphate silicate (Sr-CPS) ceramic scaffolds were prepared. The degradation, biocompatibility and bioactivity, of this Sr-doped bioceramics, were comprehensively investigated *in vitro* and *in vivo*.

2. Materials and methods

2.1. Preparation of CPS and Sr-CPS scaffolds

CPS powder was synthesized by a sol-gel method using tetraethoxysilane (TEOS), triethyl phosphate (TEP), and calcium nitrate tetrahydrate ($\text{Ca}(\text{NO}_3)_2 \cdot 4\text{H}_2\text{O}$) as sources of Si, P and Ca, respectively.

The detailed synthesis process was described in our previous study [15]. The synthesized CPS powder and various amount of SrCO_3 powder (AR, Sinopharm Chemical Reagent Co., Ltd., Shanghai, China) were mixed by ball-milling method in polyethylene bottles for 3 h. Polyethylene glycol particles were used as porogen to prepare CPS and Sr-CPS scaffolds with a porosity about 45%, while proper amount of polyvinyl alcohol (PVA) was used as a binder. Briefly, after ball-milling and drying, the mixed powders were sieved through a 200-mesh and uniaxially pressed into round specimens with dimensions of a diameter of 6 mm and a thickness of 1 mm in a stainless steel die followed by a cold isostatic pressing at 200 MPa. The pressed specimens were sintered at 1100 °C for 2 h in a muffle furnace with a heating rate of 5 °C/min. According to the mole fraction of strontium ions (5%, 10%, 20%), Sr-CPS samples were named as Sr-5, Sr-10 and Sr-20.

2.2. Sample characterization

Phase composition of the CPS and Sr-CPS samples were characterized by X-ray diffraction method (XRD, D2 Phaser, Bruker, Germany) using Cu K α radiation with a step size of 0.02° and a count rate of 5°/min. Morphologies of CPS and Sr-CPS samples were examined by scanning electron microscopy (SEM, S-3400, Hitachi, Japan). Energy-dispersive spectroscopy (EDS) was simultaneously carried out to confirm the composition of the CPS and Sr-CPS samples during the SEM observations. Molecular structures of the CPS and Sr-CPS samples were examined from 300 cm^{-1} to 1500 cm^{-1} using a Renishaw Raman spectroscopy (model inVia).

2.3. In vitro degradation

The residual mass of CPS and Sr-CPS scaffolds at different time points were measured to determine the degree of scaffolds degradation *in vitro*. Three samples were weighted (W_0) for each group and subsequently immersed in the PBS in incubators with shaking at 50 rpm at 37 °C for different periods of time. At each time point, scaffolds were collected and weighted (W_1) after freeze-drying for 2 days. The formula used to calculate the residual mass (%) was: $W_1/W_0 \times 100$ (%), where W_0 referred to the original scaffold weight and W_1 indicated degraded scaffold weight after lyophilization.

2.4. Preparation of Sr-CPS extracts

The extracts of CPS and Sr-CPS scaffolds were prepared according to the International Organization for Standardization (ISO 10993-12). Briefly, a stock solution of 200 mg/mL was first prepared by adding the granules from each ceramic scaffold into 1 M PBS buffer. After incubation at 37 °C for 24 h, the mixture was centrifuged and the supernatant was collected. Subsequently, the extract was sterilized by filtration through 0.2 μm filter membranes and stocked for further experiments. To investigate the effect of ion concentration on rBMSCs, different volume of serum-free α -MEM were added to the extracts to prepare the serial diluted extracts of 1/4, 1/8, 1/16, 1/32 and 1/64 concentrations. The concentrations of Ca, Sr and Si in the 1/16 extracts were measured using inductively coupled plasma optical emission spectroscopy (ICP-OES: 710-ES, Varian, USA).

2.5. rBMSCs culture and assays

2.5.1. rBMSCs isolation and culture

rBMSCs were obtained from the long bones of two-week-old female Sprague–Dawley (SD) rats. Briefly, after SD rats being sacrificed, bilateral femurs and tibias were harvested and all soft tissues were removed under aseptic conditions. All bone marrow was flushed from the long bones and resuspended in complete α -MEM supplemented with 10% fetal bovine serum (FBS, Gibco, U.S.A.) and 1% (v/v) penicillin/streptomycin. rBMSCs were incubated in a humidified CO_2 incubator at

37 °C. When the cells reached approximately 80% confluence, they were washed with PBS three times and then trypsinized to subculture. rBMSCs from the third passage were used for further studies.

2.5.2. rBMSCs proliferation assay

To evaluate the cytotoxic effects of the sample extracts, rBMSCs were seeded at 5×10^3 cells/well in 96-well plates. After 24 h, the culture medium was replaced with different concentrations of sample extracts. And cells were incubated at 37 °C in 5% CO₂ for 1, 4 and 7 days for the cell proliferation assay. At each time point, Cell Counting Kit-8 (CCK-8; Dojindo Molecular Technology, Japan) was used to detect the cell viability following the manufacturer's protocol. Briefly, 10% CCK-8 solution was added to each well and incubated at 37 °C for 2 h. Then, the optical density (OD) was measured at a wavelength of 450 nm using a microplate reader (Bio-Rad, Hercules, CA).

2.5.3. In vitro osteogenic differentiation assay

rBMSCs were seeded at 6×10^4 cells/well in 24-well plates at 37 °C in 5% CO₂. After 24 h of attachment, various sample extracts supplemented with 50 mM ascorbic acid, 10 mM β-glycerophosphate, and 100 nM dexamethasone (Sigma-Aldrich, USA) were used to replace the culture medium. And the media was refreshed every 2 days.

After 7 days of culture, alkaline phosphatase (ALP) staining was performed qualitatively and quantitatively to evaluate the early differentiation of rBMSCs stimulated by the sample extracts. According to the manufacturer's protocol, cells were fixed with 4% paraformaldehyde and stained by making use of an ALP microplate test kit (Nanjing Jiancheng Bioengineering Institute, Nanjing, China). Briefly, after being lysing with 1% TritonX-100 (Beyotime, China), the lysates of the samples were transferred to a centrifuge tube and centrifuged for 10 min at 4 °C (12 000 rpm) to obtain the supernatants. The total protein was measured by a Bicinchoninic acid (BCA) Protein Assay Kit (Thermo Scientific, USA) and the results were normalized to the total protein.

After 21 days of culture, alizarin red staining was performed to determine the extracellular matrix mineralization of rBMSCs stimulated by different sample extracts. In brief, after fixing with 4% paraformaldehyde for 20 min at 37 °C, cells were stained with 1% alizarin red solution (Sigma-Aldrich, USA) for 30 min at room temperature. Ultrapure water was used to remove uncombined dyes totally. For quantitative analysis of Alizarin Red staining, 10% cetylpyridinium chloride (C9002-25G; Sigma-Aldrich, USA) was used to elute mineralized nodules. The absorbance of the resulting solution at 562 nm was determined by a microplate reader (Bio-Rad, Hercules, CA).

After incubated with osteogenic-inducing medium containing CPS or Sr–CPS extracts for 4 and 7 days, Quantitative real-time polymerase chain reaction (qRT-PCR) assay was performed to evaluate osteogenic gene expression (RUNX2, OCN, OPN, BSP) of rBMSCs. Total RNA was extracted using Trizol reagent (Invitrogen, U.S.A.). Following the manufacturer's protocols, the isolated RNA was reverse transcribed into cDNA by using a Prime-Script™ RT reagent kit (Takara Bio, Shiga, Japan). Transcription-PCR was performed with real-time PCR (ABI 7500; Applied Biosystems, Foster City, CA) and the relative gene expressions were calculated by the $2^{-\Delta\Delta Ct}$ method.

2.6. Bone marrow monocytes (BMMs) culture and assays

2.6.1. BMMs isolation, culture and proliferation assay

BMMs were obtained from bilateral femurs and tibias of 6-week-old C57/BL6 mice. The bone marrow was flushed by complete α-MEM containing 30 ng/mL macrophage colony-stimulating factor (M-CSF, Pepro Tech, Rocky Hill, NJ). BMMs were cultured in a 5% CO₂ incubator at 37 °C and the culture medium were changed every day. When the cells reached approximately 80% confluence, those cells were washed with PBS three times and then trypsinized for further studies. As described above, CCK-8 was also used to evaluate the cytotoxic

effects of the sample extracts on BMMs.

2.6.2. In vitro osteoclastogenesis assays

BMMs (1.5×10^4 cells/well) were plated and incubated in 96-well plates in triplicate. After 24 h, the medium was replaced by complete α-MEM supplemented with 30 ng/mL macrophage colony-stimulating factor (M-CSF, Pepro Tech, Rocky Hill, NJ), 50 ng/mL recombinant mouse receptor activator of nuclear factor-κB ligand (RANKL, R&D) and different sample extracts for osteoclast differentiation. The culture medium was changed every day and the cells were fixed by 4% paraformaldehyde for tartrate-resistant acid phosphatase (TRAP) staining using the TRAP staining kit (387A-1 KT; Sigma-Aldrich) at day 7. The numbers and the size of TRAP-positive cells in each well were calculated by Image-Pro Plus software (Media Cybernetics, Bethesda, MD).

The recruitment of TRAF6 caused by interaction between RANKL and RANK (receptor activator of nuclear factor-κB) leads to the activation of multiple critical signaling pathways [23]. These signaling pathways induce NFATc1, a key transcription factor which plays an important role in osteoclastogenesis. Furthermore, NFATc1 can promote the expression of a variety of osteoclastogenesis-related genes, including TRAP, MMP 9, CFOS, Cathepsin K [24]. The expressions of these genes were determined by qRT-PCR. Briefly, BMMs were seeded in a six-well plate at a density of 2×10^5 cells/well. After BMMs were incubated with osteoclastic-inducing medium containing CPS or Sr–CPS extracts for 4 and 7 days, qRT-PCR assay was performed to evaluate osteoclastogenesis-related gene expression (TRAP, TRAF6, MMP 9, CFOS, NFATc1, Cathepsin K) as described previously.

2.7. Molecular mechanism evaluation

Western blot (WB) analysis was performed to study the molecular mechanism regulated by CPS or Sr-CPS extracts. Sr-20 was selected as the typical material to represent the Sr-CPS.

For the osteogenic mechanism, rBMSCs were seeded in a six-well plate at a density of 2×10^5 cells/well and cultured in osteogenic-inducing medium containing CPS or Sr–CPS extracts for 7 days. For the osteoclastic mechanism, BMMs were seeded in a six-well plate at a density of 4×10^5 cells/well and cultured in osteoclastic-inducing medium containing CPS or Sr–CPS extracts for 30 min. At each time point, total protein was extracted from rBMSCs and BMMs using RIPA (Beyotime) lysis buffer and concentrations of the total protein were analyzed by a BCA protein assay kit (Thermo Scientific). Twenty μg of proteins from each group were separated using 10% SDS-PAGE gel electrophoresis and then transferred to PVDF membranes. Then the membranes were blocked by 5% dried nonfat milk for 2 h at room temperature and incubated overnight at 4 °C with each primary antibodies (CST, U.S.A.). Furthermore, the membranes were incubated with HRP-conjugated secondary antibody (CST, U.S.A.) for 1 h. The protein bands were visualized by Odyssey imaging system (Li-Cor, Lincoln, NE) and quantitative analysis was carried out by ImageJ software.

2.8. In vivo experiments

2.8.1. Animal and surgical procedure

All the animal experiment procedures were performed under the authorization of the Animal Care and Experiment Committee of the Ninth People's Hospital Affiliated to Shanghai Jiao Tong University School of Medicine (Shanghai, China). Thirty-six female Sprague-Dawley rats, aged 6 months (SLAC Laboratory Animal Co., Ltd., Shanghai, China), were used in this study to build osteoporotic bone defect model. Firstly, ovariectomy (OVX) was performed to generate animal models for postmenopausal osteoporosis. Then, three months after ovariectomy, bilateral bone defects were made on calvarium. Briefly, rats were anaesthetized by intraperitoneal injection of 1% pentobarbital sodium (100 mg/kg). A 1.5 cm sagittal incision was made on the scalp and the skull was exposed slowly. Furthermore, a 5-mm

diameter trephine bur was applied to make bilateral critical-sized defects. CPS and Sr-CPS ceramic scaffolds were used to randomly fill the defects. The incisions were closed in layers, and prophylactic antibiotic was administered to avoid infections. At eight weeks post-operation, the rats were sacrificed by the lethal dose of pentobarbital sodium.

2.8.2. Micro-computed tomography (Micro-CT) measurement

To compare the osteogenic capacity between CPS and Sr-CPS scaffolds, Micro-CT (μ CT 80; SCANCO Medical AG, Bassersdorf, Switzerland) were performed to evaluate bone defect healing and scaffolds degradation. Firstly, rat calvariums were harvested and fixed in 4% neutral-buffered formalin for 48 h. Secondly, the specimens were scanned with following parameters: voltage, 70 kV; electric current, 114 μ A; and resolution of 10 μ m per pixel. After scanning, three-dimensional (3D) image was reconstructed. Bone mineral density (BMD), bone volume/total tissue volume (BV/TV), trabecular number (Tb.N) and trabecular thickness (Tb.Th) in the bone defect were analyzed by using its auxiliary software (Scanco Medical AG, Switzerland).

2.8.3. Histological staining and histomorphometric analysis

After micro-CT scanning, the calvarial samples were decalcified in 10% EDTA (pH = 7.4) for 3 weeks and then embedded in paraffin. For microstructure observation, four longitudinal sections (150 μ m thick) of each specimen were prepared for hematoxylin and eosin (H&E), TRAP, Masson-trichrome and Immunohistochemical (IHC) stainings. IHC staining was accomplished with antibodies against ALP and RUNX-2 (USA, Affinity; dilution 1:100). The images were obtained using a high-quality microscope (Leica DM4000B).

2.9. Statistical analysis

All data are presented as the mean \pm standard deviation (SD). Differences between the experimental and control groups were evaluated by Student's t-test. One-way analysis of variance (ANOVA) was used for multifactorial comparisons in this study. A P value < 0.05 was considered as statistically significant. * and # indicate P < 0.05, ** and ## indicate P < 0.01. All data analysis was conducted using SPSS 22.0 analysis software (SPSS Inc, Chicago, IL).

3. Results

3.1. Scaffolds characterization

The cross-section view of CPS and Sr-CPS samples was shown in Fig. 1A. It could be seen that all the CPS and Sr-CPS scaffolds have ultrafine microstructure. In addition, it could also be noted that there were many nano pores existed in the scaffolds which might be caused by the decomposition of residual organic phase in CPS.

Fig. 1B showed the XRD patterns of CPS and Sr-CPS samples sintered at 1100 °C. It could be seen that the diffraction pattern of CPS powders was coincided well with the data of PDF #40–393, indicating a crystallized silicocarnotite phase. It seemed no extra Sr compounds were detected. With an increase of Sr substitution, the diffraction peaks of CPS shifted to lower 2 theta values, which indicated the substitution of Ca ions by Sr ions, since Sr²⁺ (0.118 nm) has a larger radius than Ca²⁺ (0.1 nm). Furthermore, the diffraction intensity of Sr-CPS samples decreased and the peaks broadened with an increase of Sr content, which was due to the expansion of CPS network caused by the solid solution of Sr.

The EDS analyses of CPS and Sr-CPS samples were shown in Table 1. It was evident to see that with the increase of Sr, the content of Ca decreased. The content of other elements (O, P and Si) in Sr-5 and Sr-10 samples had no great difference compared to CPS sample. Combined with XRD and EDS results, it could be confirmed that Sr ions were doped into the CPS structure.

The Raman spectra of CPS and Sr-CPS scaffolds were showed

Fig. 1C. As a general observation, the spectra seemed quite similar, indicating the structure of the CPS and Sr-CPS was not changing greatly with strontium substitution for calcium. The asymmetric band in (Fig. 1C) around 847 cm⁻¹ was due to the vibrations of inter-tetrahedral Si–O–Si while the orthophosphate vibration at around 950 cm⁻¹ could be seen which corresponded to the symmetric stretch of P–O [25]. The band position and line shape changed slightly with strontium substitution. This was likely due to the influence of strontium, which expanded the CPS network, and would change the Si–O and P–O band distances and angles [26]. The position of the peak shifted to lower wavenumbers with increasing Sr addition to CPS sample. This was consistent with the observation in a series of Sr–Ca-hydroxyapatites previously reported in the literature indicating a red-shift in frequency with increased association of the orthophosphate groups with a heavier ion (Sr) [27]. In summary, the Raman spectroscopic data agreed with the XRD analysis; the CPS structure did not change significantly after adding strontium, even at a substitution of 20 mol % for calcium.

3.2. In vitro degradation

The residual mass of different scaffolds after different cultivation time is presented in Fig. 2C. All the scaffold degraded gradually during the experiment period. After a 21-day experiment, the residual mass of CPS, Sr-5, Sr-10 and Sr-20 scaffold were 74.7 \pm 0.4%, 69.4 \pm 3.3%, 65.3 \pm 1.3% and 54.4 \pm 4.2%. Sr-CPS scaffolds showed a significantly increased degradation rate. Furthermore, with the increase of Sr content, the scaffold degradation rate gradually increased.

3.3. Effect of CPS and Sr–CPS extracts on rBMSCs proliferation

Cell proliferation is important in evaluating the scaffolds biocompatibility. According to CCK-8 results (Fig. 2A), rBMSCs showed robust proliferation in different concentrations of CPS or Sr-CPS extracts throughout the assay period. In general, the addition of Sr ion in Sr-CPS extracts significantly enhanced rBMSCs growth at day 4 and day 7 compared with CPS and rBMSCs exhibited highest vitality in 1/16 group. At day 4, 1/16 and 1/32 group showed higher OD values. At day 7, compared with 1/32 group, 1/16 group showed a stronger stimulatory effect on cell proliferation. Therefore, the 1/16 group was used in the following study due to its highest proliferation.

The concentration of Ca, Si and Sr ions of CPS and Sr-CPS samples from 1/16 dilution was shown in Fig. 2B. The Ca ions concentration was increased with the adding of Sr content except Sr-20 sample, while Si ion concentration was decreased with the existence of Sr ions. There was no doubt that with an increase of Sr content, the Sr ions concentration was increased. It could be concluded that the presence of Sr ions in the CPS structure hindered the release of Si ions.

3.4. The stimulation of sample extracts on osteogenic differentiation of rBMSCs

ALP activity is widely used as an early marker of early osteogenic differentiation. rBMSCs cultured in different sample extracts and osteogenic medium alone were fixed and stained. As shown in Fig. 3A, CPS and Sr-CPS both enhanced the ALP activity at day 7. Sr-CPS showed more intensive ALP staining. The quantitative analysis (Fig. 3B) indicated Sr-5, Sr-10 and Sr-20 enhanced the activity of ALP compared with that of CPS. Both Sr-10 and Sr-20 owned significantly higher activity than Sr-5 but there was no statistically significant difference between these two groups. At day 21, semi-quantitative analysis of alizarin red staining (Fig. 3C) also prove Sr-20 group had the strongest osteogenic capacity. The quantitative results of ALP expression coincided well with the alizarin red staining results.

According to the results of qRT-PCR (Fig. 4A), osteogenesis-related gene expression such as RUNX2, OCN, OPN and BSP were upregulated in Sr-CPS and CPS in comparison with the control group at days 4 and 7.

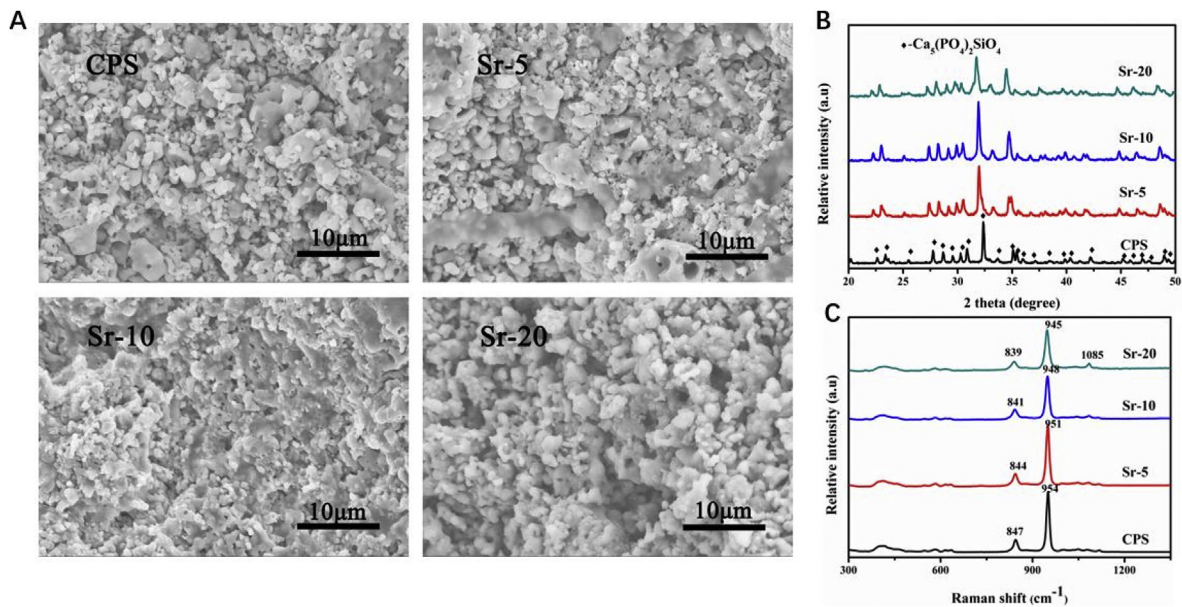


Fig. 1. (A) Cross-section view of CPS and Sr-CPS scaffold; (B) XRD patterns of CPS and Sr-CPS samples; (C) Raman spectra of CPS and Sr-CPS scaffold.

Table 1
The element composition (%) of CPS and Sr-CPS sample.

Element composition (%)	O	P	Ca	Si	Sr
CPS	53.6	19.5	20.4	5.8	–
Sr-5	55.9	18.3	18.9	5.3	1.6
Sr-10	55.3	18.3	18.1	5.7	3.3
Sr-20	56.7	18.1	14.7	4.5	6.0

Furthermore, the Sr–CPS groups had a markedly increased effect of osteogenesis compared with the CPS group at each time point. These four gene expression profiles showed the similar tendency. The ALP staining, alizarin red staining and qRT-PCR experiments showed that both CPS and Sr-CPS promoted rBMSCs osteogenic differentiation, while Sr-CPS exhibited stronger stimulatory effect especially Sr-20.

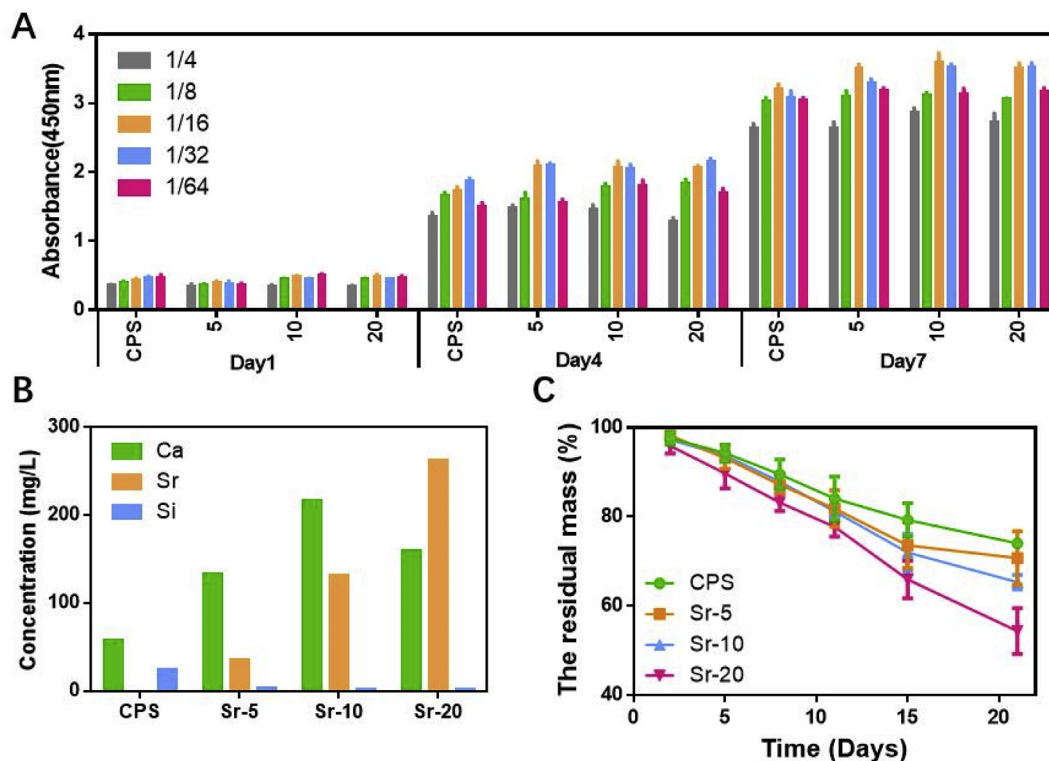


Fig. 2. (A) rBMSCs cultured with different concentrations of ceramics extracts; (B) Ca, Si, Sr concentration of CPS and Sr-CPS samples from 1/16 dilution; (C) *In vitro* degradation of CPS and Sr-CPS scaffolds.

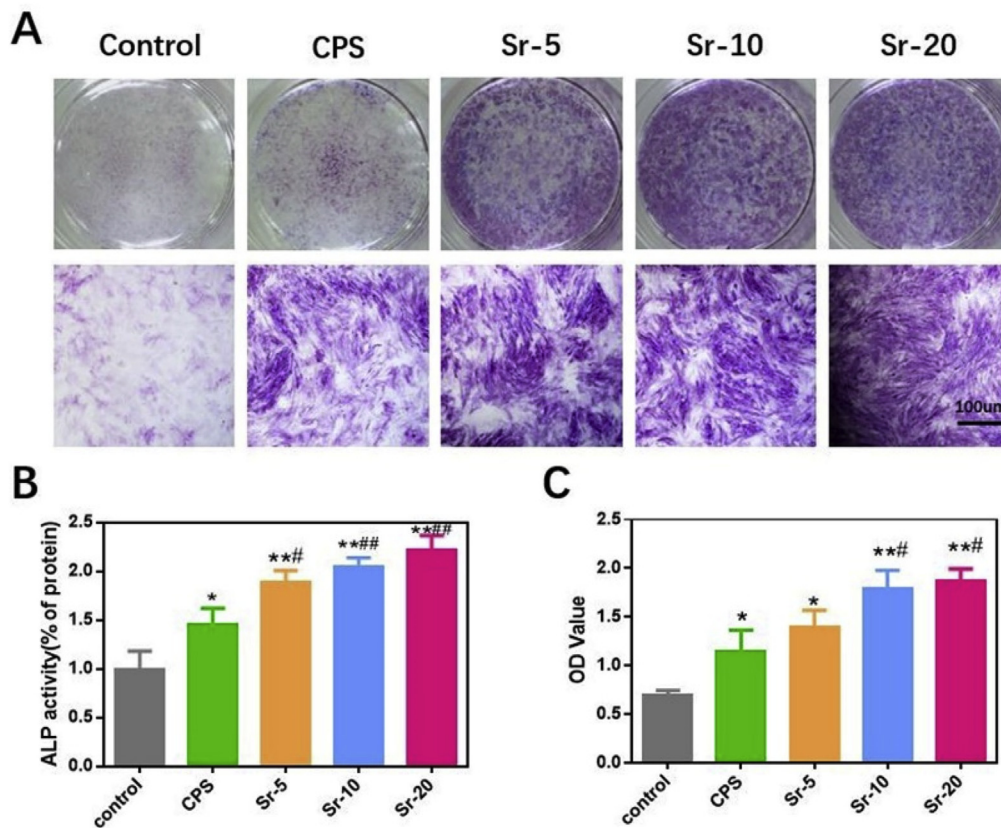


Fig. 3. (A) ALP staining of rBMSCs at day 7; (B) Quantification of the ALP staining; (C) Semi-quantitative analysis of the alizarin red staining at 21 days. * Compared with the control group; # compared with CPS group.

3.5. Sr-CPS enhanced osteoblastogenesis through the Wnt/ β -catenin pathway

Wnt/ β -catenin signaling pathway was reported to play an important role in bone development and homeostasis [28]. The canonical Wnt signaling is closely related to rBMSCs osteogenic differentiation [29]. The stability of β -catenin is regulated by glycogen synthase accumulation of β -catenin in the cytoplasm [30]. Therefore, Wnt/ β -catenin Signaling Pathway could be activated by inhibition of GSK3 β . As indicated in Fig. 4B and C, western blotting analysis showed that CPS and Sr-CPS extracts drastically induced upregulation of GSK3 β phosphorylation and β -catenin. And the expression of the critical osteoblast transcription factor RUNX2 was also promoted in osteoprogenitor cells. Furthermore, Sr-CPS showed a significant increase in phosphor-GSK3 β expression in comparison with CPS.

3.6. The inhibition of sample extracts on cells osteoclastic differentiation

First, according to CCK-8 assays (Fig. 5B), both CPS and Sr-CPS extracts were not cytotoxic to BMMs compared with osteoclastic-inducing medium.

The effect of Sr-CPS on RANKL-induced osteoclastic differentiation *in vitro* was studied firstly. The number and size of TRAP-positive multinucleate cells are signs to evaluate the extent of osteoclast differentiation. As shown in Fig. 5A., numerous TRAP-positive multinucleate osteoclasts were found in the control group and CPS group. No significant difference was found between these two groups. However, Sr ions suppressed osteoclast formation in a dose-dependent manner. As the concentration of Sr ions increased, the inhibition effect on osteoclast activity also gradually enhanced, and significant differences between adjacent groups were found. These results indicated that the supplementation of Sr ions provided CPS scaffold with the ability to

inhibit the osteoclastic differentiation of BMMs.

Specific signaling pathways affect cell osteoclast differentiation and alter their gene expression. Osteoclast-related genes expression, including TRAF6, TRAP, NFATc1, c-Fos, Cathepsin K, and MMP9, was evaluated using qRT-PCR to further study the mechanism behind the inhibitory effect of Sr-CPS on osteoclasts. From results of qRT-PCR (Fig. 6A), it was found that the supplementation of Sr ions remarkably suppressed NFATc1 and thus down-regulated related genes. This effect was dose-dependently and the results were consistent with the TRAP staining. As a comparison, no significant difference was found between CPS and the control, which indicated that CPS had no obvious effect on osteoclastogenesis.

3.7. Sr-CPS inhibited osteoclastogenesis through the NF- κ B pathway

When RANKL binds to its receptor RANK, tumor-necrosis factor (TNF) receptor-associated factor 6 (TRAF6) will be activated thus stimulating the NF- κ B pathway [31,32]. NF- κ B is reported to be important for osteoclast development, function and survival [33]. Hence, NF- κ B pathway related protein expression was detected through western bolt assay.

The quantitative results (Fig. 6C) showed that I κ B α of Sr-CPS group was significantly up-regulated in comparison with CPS samples. And a down-regulation of phosphorylation-P65 was also found. It confirmed that Sr-CPS acted on I κ B α and decreased the downstream phosphorylation of P65. Noticeable, no significant difference was found between the CPS and control group, which was consistent with the previous osteoclast assays and further demonstrated that the addition of Sr ions in CPS made it possible to inhibit osteoclast activity by suppressing the NF- κ B pathway.

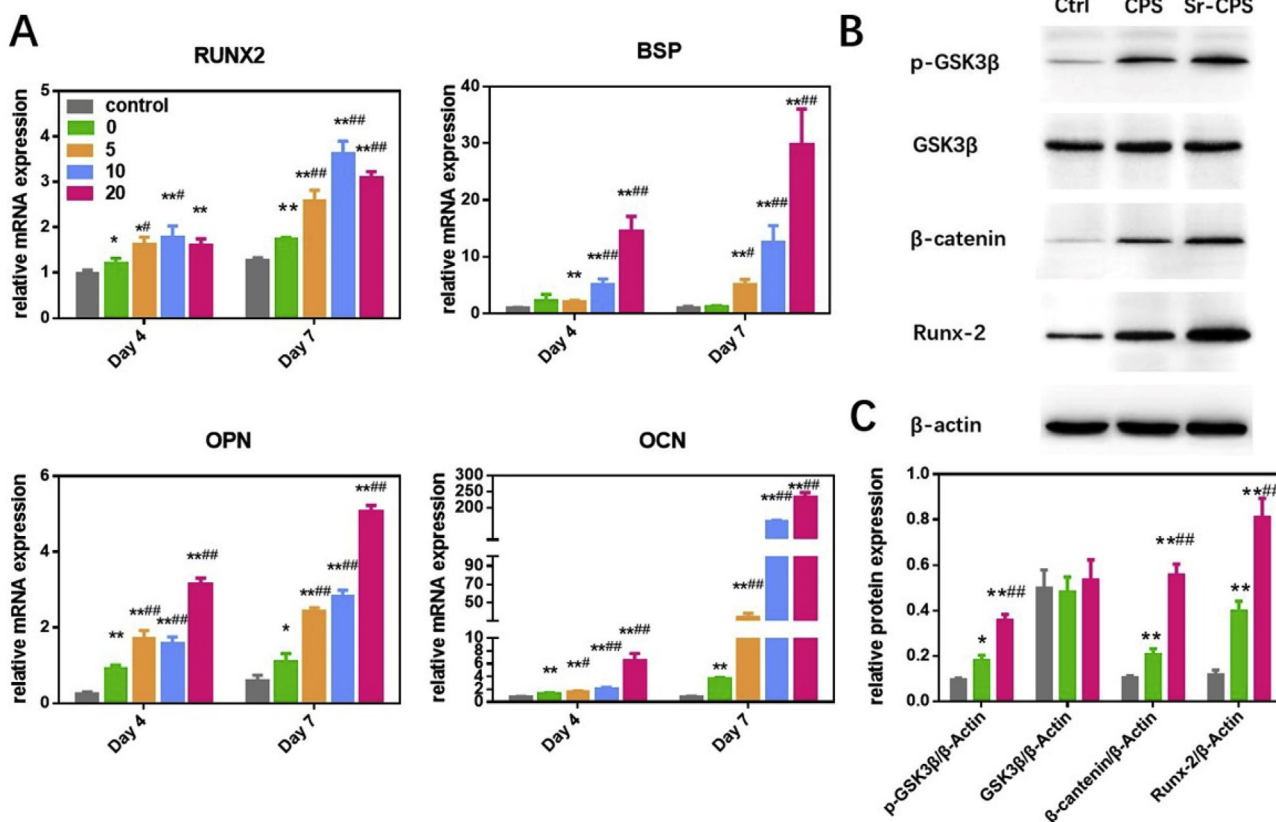


Fig. 4. (A) Expression of the osteogenesis-specific genes including RUNX2, BSP, OPN and OCN; (B) Western blotting showed that Sr-CPS affected the Wnt/ β -catenin pathway-related proteins GSK3 β , p-GSK3 β , β -catenin and RUNX-2; (C) Quantification of the Western blotting. * Compared with the control group; # compared with CPS group.

3.8. In vivo studies

3.8.1. Micro-CT results

In vivo, Micro-CT and histology analyses further approved that Sr incorporated CPS scaffolds had significantly positive effects for bone

defect healing in an osteoporotic animal model. As shown in Fig. 7A, the cross-sectional images showed the morphology of the newly formed bone calluses in Sr-CPS groups were much larger compared with those in the CPS group at 8 weeks post-operation. The 3D-reconstructed micro-CT (Fig. 7B) at 8 weeks post-operation revealed that Sr-CPS

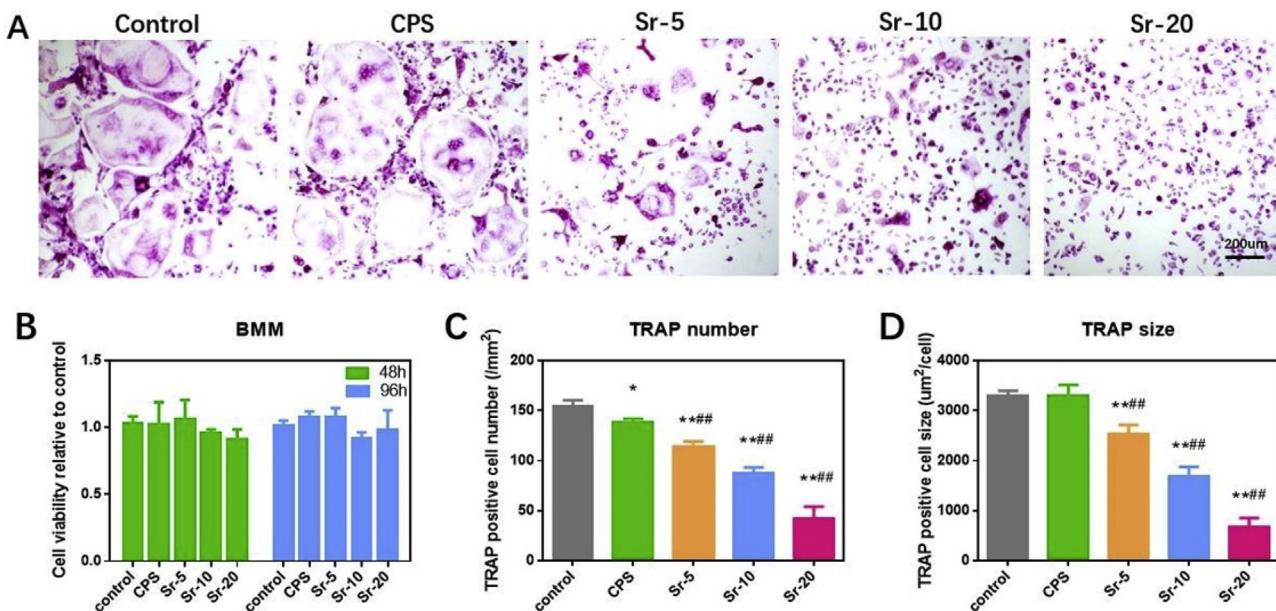


Fig. 5. (A) TRAP staining of osteoclasts at day 7; (B) Bone marrow macrophages (BMMs) were treated with different extracts and analyzed using CCK-8 assays; (C,D) Quantification of the number and size of osteoclasts. * Compared with the control group; # compared with CPS group.

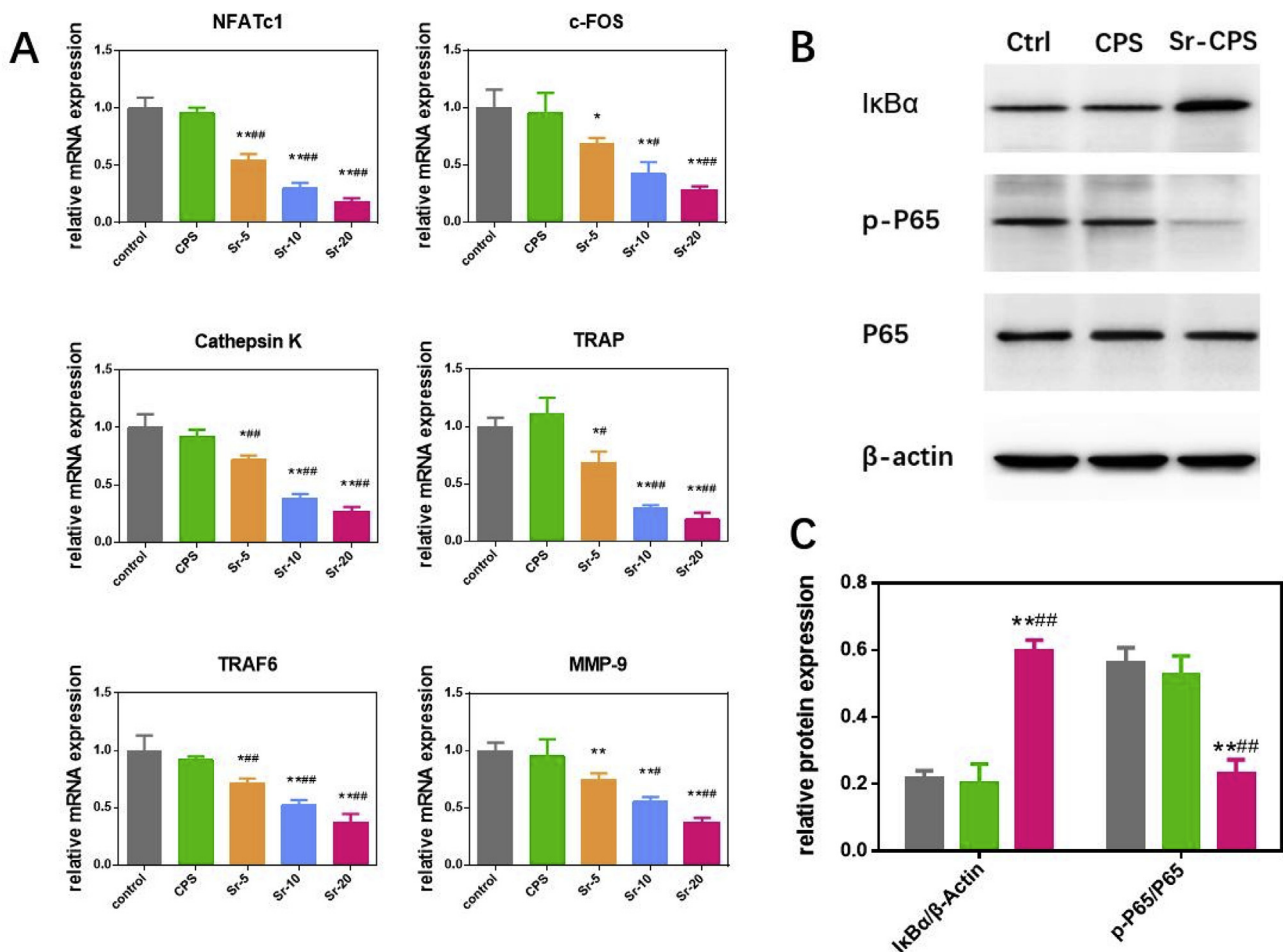


Fig. 6. (A) Expression of the osteoclast-specific genes including NFATc1, Cathepsin K, TRAF6, c-FOS, TRAP and MMP-9; (B) Western blotting showed that Sr-CPS affected the NF- κ B pathway-related proteins I κ B α , P65 and p-P65; (C) Quantification of the Western blotting. * Compared with the control group; # compared with CPS group.

scaffolds were covered by more new bones and achieved higher new bone colonization compared with the CPS scaffold. Furthermore, the degradation rate of the scaffold gradually accelerated as the content of strontium increased. In Fig. 7D, Sr-20 showed the fastest degradation rate and the volume of un-degraded scaffold was 42.9%. Three-dimensional reconstructed images of 8 weeks after surgery showed more space became available for new bone ingrowth as the Sr-20 and Sr-10 scaffolds degraded.

Histomorphometry analysis of the callus tissue revealed that the order of values of bone volume/total volume ratio (BV/TV) and bone mineral density (BMD) was: Sr-10 > Sr-20 > Sr-5 > CPS. Implantation of the Sr-CPS led to significantly improved BV/TV and BMD in comparison with the CPS group (Fig. 7D). Significant differences of BMD and BV/TV were found between Sr-5 and CPS group. In addition, Sr-10 showed the best bone healing with the highest BMD, BV/TV, trabecular number (Tb.N) and trabecular thickness (Tb.Th).

3.8.2. Histological analysis

An osteogenic histological assessment of the Sr-CPS and CPS samples was carried out 8 weeks after the rat calvarial defect operation. H&E and Masson staining were conducted in bone sections to assess the healing of bone defects. In H&E staining (Fig. 8A), CPS had more residual scaffold than Sr-CPS. In CPS group, less new bone was found and the defect was occupied mainly by fibrous tissue at 8 weeks post-operation. On the contrary, the addition of Sr ions greatly improved the bone formation, especially the Sr-10 sample. From the region of the interface between bone and scaffold (Fig. 8B), it was found that Sr-CPS

promoted the formation of mature bone, as well as induced new bone formation in the defect. In Masson staining (Fig. 9A.), the red color indicates host bone or newly formed bone and osteoid tissues while the blue represents fibrous tissue or freshly formed bone [34]. Compared with CPS group, more blue tissues were found inside the scaffolds in Sr-CPS groups which indicated better bone ingrowth. More blue tissue was also found at the interface between bone and Sr-CPS scaffolds, indicating that the addition of Sr ions obviously improved the tissue compatibility of the CPS. Additionally, at week 8, the ALP and RUNX-2 immunohistochemical (IHC) staining (Fig. 9C&D) also demonstrated the osteogenic capacity of Sr-CPS. Consistent with the previous assays, more ALP or RUNX-2 positive cells were found in Sr-CPS groups. Sr-10 group showed more positive cells than other groups, however, no significant difference was found between it and Sr-20.

The TRAP staining was used for osteoclastic histological evaluation. As shown in Fig. 9B, more osteoclasts were found in the CPS group, while the trap-positive cells decreased dose-dependently after implanted with Sr-CPS. This result indicated that the addition of Sr ions was also effective in inhibiting osteoclast activity *in vivo*.

3.9. Discussions

The balance between the bone-forming osteoblasts and bone-resorbing osteoclasts is critical for bone homeostasis [35]. In osteoporosis, this balance is destroyed by overactivation of osteoclasts and defective osteoblast activity [36]. Therefore, treatments for osteoporosis aim to reverse this imbalance. However, it is difficult to

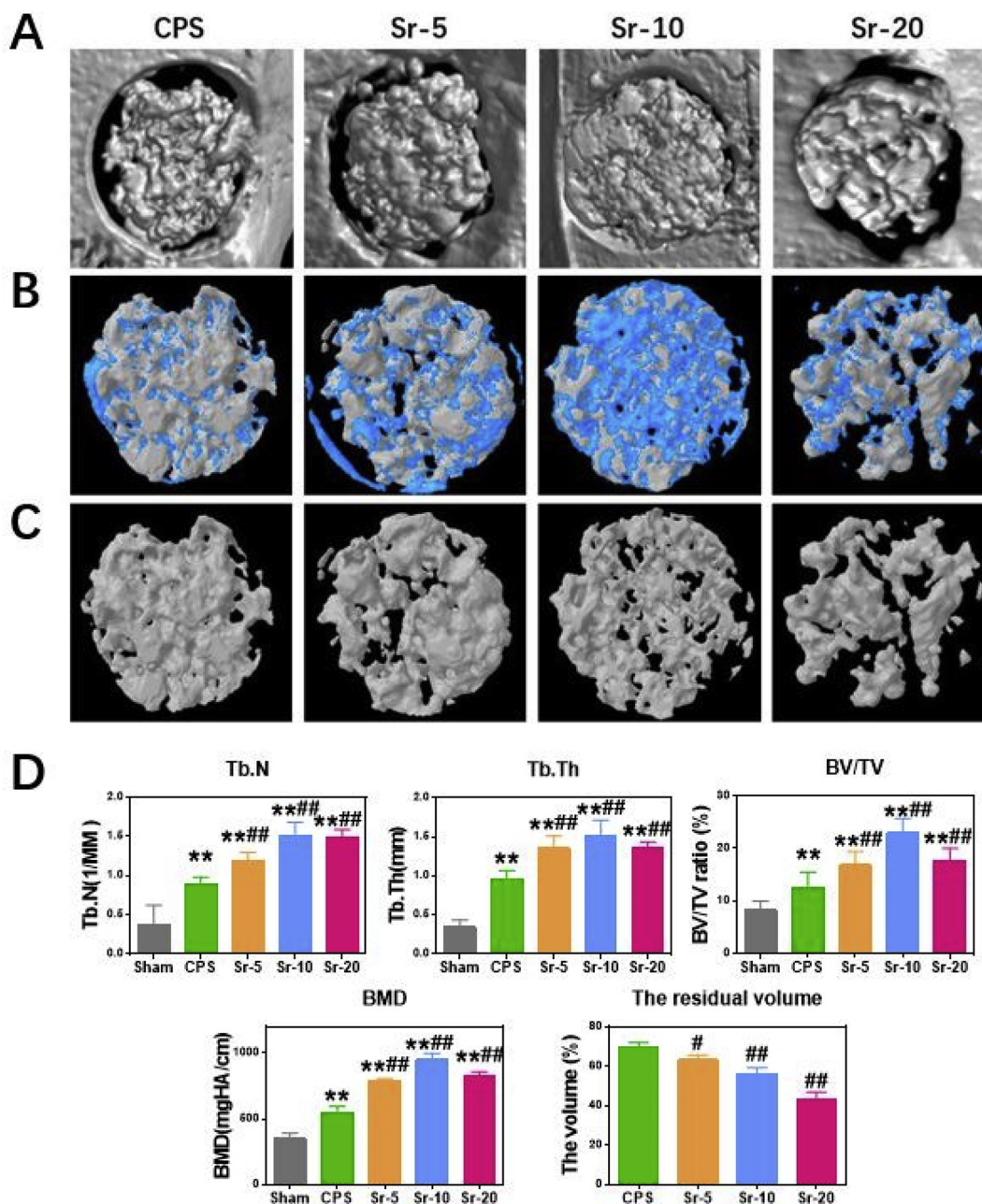


Fig. 7. (A) Micro-CT evaluation of the repaired skull after 8 weeks of implantation, (B) 3d-reconstruction images of Micro-CT. The blue part was the new bone and the white was the scaffold, (C) 3d-reconstruction images of residual scaffolds (scale bar = 1.5 mm), (D) Morphometric analysis of Micro-CT, including BMD, Tb.N, Tb.Th, BV/TV and the residual volume of scaffolds.* Compared with Sham group; # compared with CPS group.

enhance osteogenesis and inhibit osteoclastogenesis at the same time due to the couple effects of these two processes. For example, bisphosphonates, a class of drugs for bone disorders, can target bone degradation by disrupting protein prenylation via inhibition farnesyl pyrophosphate synthase (FDPS), but also impair osteoblast activity [37]. Similarly, a parathyroid-hormone-related peptide (PTHrP)-analogue, approved by the FDA in April 2017, is effective on promoting bone formation, but also strengthen osteoclast activity [38]. Moreover, when the drug administered systemically, it is difficult for them to achieve effective local concentration at the fracture or defect site and they may be insufficient for stimulating bone regeneration. Hence, dual action therapeutic biomaterials which can suppress bone resorption and enhance bone formation simultaneously are urgently needed for osteoporosis bone defect. In recent years, CPS, a novel bioceramic, has attracted much attention for its superior cytocompatibility and

osteogenic activity [11].

Strontium is a mineral that is absorbed in the body like calcium. Sr in the form of strontium ranelate (SrR) was proved to have the ability to increase bone formation while inhibiting osteoclast differentiation and has been used for the treatment of osteoporosis for decades [39]. Because of the positive effects of Sr ions on bone regeneration, Sr-containing biomaterials have gained interests among researchers. Lin et al. has proved Sr-substituted calcium silicate ceramic scaffolds dramatically stimulated bone regeneration and angiogenesis in an osteoporosis rat model [40]. In another novel research, Naruphontjirakul et al. successfully fabricated a novel strontium containing bioactive glass nanoparticles, and found their ionic release products had the potential to promote bone formation [41]. Based on the hypothesis that the addition of Sr may endow CPS with anti-osteoclast ability and enhanced osteogenic effect, a biodegradable Sr-CPS scaffold was designed and

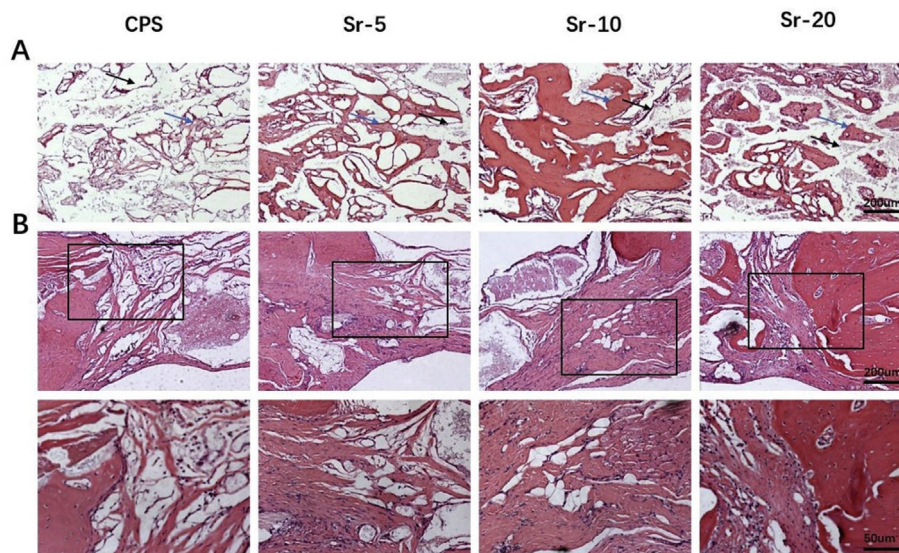


Fig. 8. H&E staining. (A) Defect sites at weeks 8 after operation: the new bone formation (blue arrows) and residual scaffold (black arrows), (B) The interface between bone and scaffold. (40x & 100x).

fabricated in the present work, which was expected to have specific effects for osteoporotic bone defect repair.

As a bone regeneration implant, favorable biocompatibility is the basic requirement. *In vitro*, a proper concentration of Sr-CPS was chosen according to CCK-8 assays. In different concentration groups, rBMSCs proliferated apparently over time throughout the 7-day period, indicating that CPS and Sr-CPS extracts had no negative effect on cell proliferation. Previous study has confirmed that Sr ions could promote rBMSCs proliferation as well as the osteogenic differentiation [42]. However, a study indicated that excessive strontium content of implants could negatively affected the osteoblast proliferation [43]. In this study, the results indicated 1/16 extract concentrations had a remarkably positive effect on rBMSCs proliferation and 1/16 was chosen for *in vitro* assays in the present work. The ALP staining, AR staining and qRT-PCR experiments showed that both CPS and Sr-CPS promoted rBMSCs osteogenic differentiation, while Sr-CPS exhibited stronger stimulatory effect especially Sr-20. Moreover, Sr-CPS dramatically inhibited osteoclastogenesis. In general, Sr-CPS demonstrated excellent promoting osteogenesis and anti-osteoclastogenesis functions *in vitro*, and these effects were dose-dependent with Sr ion concentration.

In vivo, Micro-CT and histology analyses further approved that Sr incorporated CPS scaffolds had significantly positive effects for bone defect healing in an osteoporotic animal model. An ideal scaffold must own a proper degradation rate to provide a space and a long-term structure support for new bone formation [44]. Few studies have focused on the degradation of strontium-containing bioceramics in osteoporotic animals. As shown in Figs. 2C & 7C, the supplementation of Sr ions accelerated the degradation of CPS. Additionally, the degradation rate increased monotonically with the increase of strontium content. On the other hand, Tb.TH, Tb.N, TV/BV and BMD had similar trends: gradual increase with the addition of Sr ions but a sharp reduction in Sr-20 group. It could be seen that the CPS and Sr-5 scaffolds showed a limited bone formation ability, while, Sr-20 exhibited a faster degradation rate than bone formation rate although the *in vitro* extract results showed the best performance. The previous work has also verified that too much osteoclast inhibition may have a negative effect on bone remodeling and tissue regeneration [18]. Sr-10 sample showed a perfect match of bone formation and degradation rates.

In CPS group, the degradation of scaffold was retarded and there was not enough space for bone ingrowth. Bone reconstruction was also limited due to the insufficient bioactivity. Sr-20 degraded fastest,

however, premature degradation also led to insufficient mechanical support for bone reconstruction. In comparison, Sr-10 exhibited a relatively appropriate degradation rate to induce bone regeneration within the defective area at 8 weeks post-operation. The *in vivo* results were inconsistent with those observed *in vitro*: Sr-10 replaced Sr-20 as the best performing scaffold. Therefore, the moderate amount of Sr incorporated in Sr-10 helped it find a balance between bone formation and bone resorption, leading to its outstanding performance in an osteoporotic animal model.

Several signaling pathways have been shown to be related to bone formation. Many studies have confirmed that Wnt/ β -catenin signaling pathway plays a significant role in promoting osteoblast differentiation [45]. When this signaling is activated, Wnt proteins bind to frizzles and co-activate with co-receptors and the cytoplasmic GSK3 β complex is destroyed. Subsequently, degradation of β -catenin is prevented and the accumulated β -catenin enters the nucleus as well as activates target genes. In our study, CPS was found to stimulate the phosphorylation of GSK3 β . Thereafter, the nuclear translocation of β -catenin and nuclear expression of RUNX2 was also promoted. The results of WB demonstrated that CPS effectively promoted osteogenesis through the activation of Wnt/ β -catenin signaling pathway. Furthermore, the addition of Sr ions amplified this effect. In osteoporosis, overactive osteoclastogenesis is closely associated with delayed healing of bone defect. The classical NF- κ B pathway regulates the expression of osteoclastogenesis related genes [46]. Our study found that Sr-CPS had significant inhibitory effect on the phosphorylation of NF- κ B subunit P65 by promoting the expression of I κ B α . NFATc1 is a key transcription factor which can regulate the expression of many genes related to osteoclast differentiation and function [24]. From results of qRT-PCR, it was found that the supplementation of Sr ions remarkably suppressed NFATc1 and thus down-regulated related genes, such as c-FOS, TRAP, MMP-9, Cathepsin K and TRAF6. As a comparison, no significant difference was found between CPS and the control, which indicated that CPS has no obvious effect on osteoclastogenesis. In general, *in vitro* and *in vivo* assays indicated that accelerated healing of osteoporosis bone defect could be achieved with the Sr-CPS scaffold due to the combination of promoting osteogenesis and anti-osteoclastogenesis functions.

4. Conclusions

This study showed the beneficial effects of Sr-CPS in treating

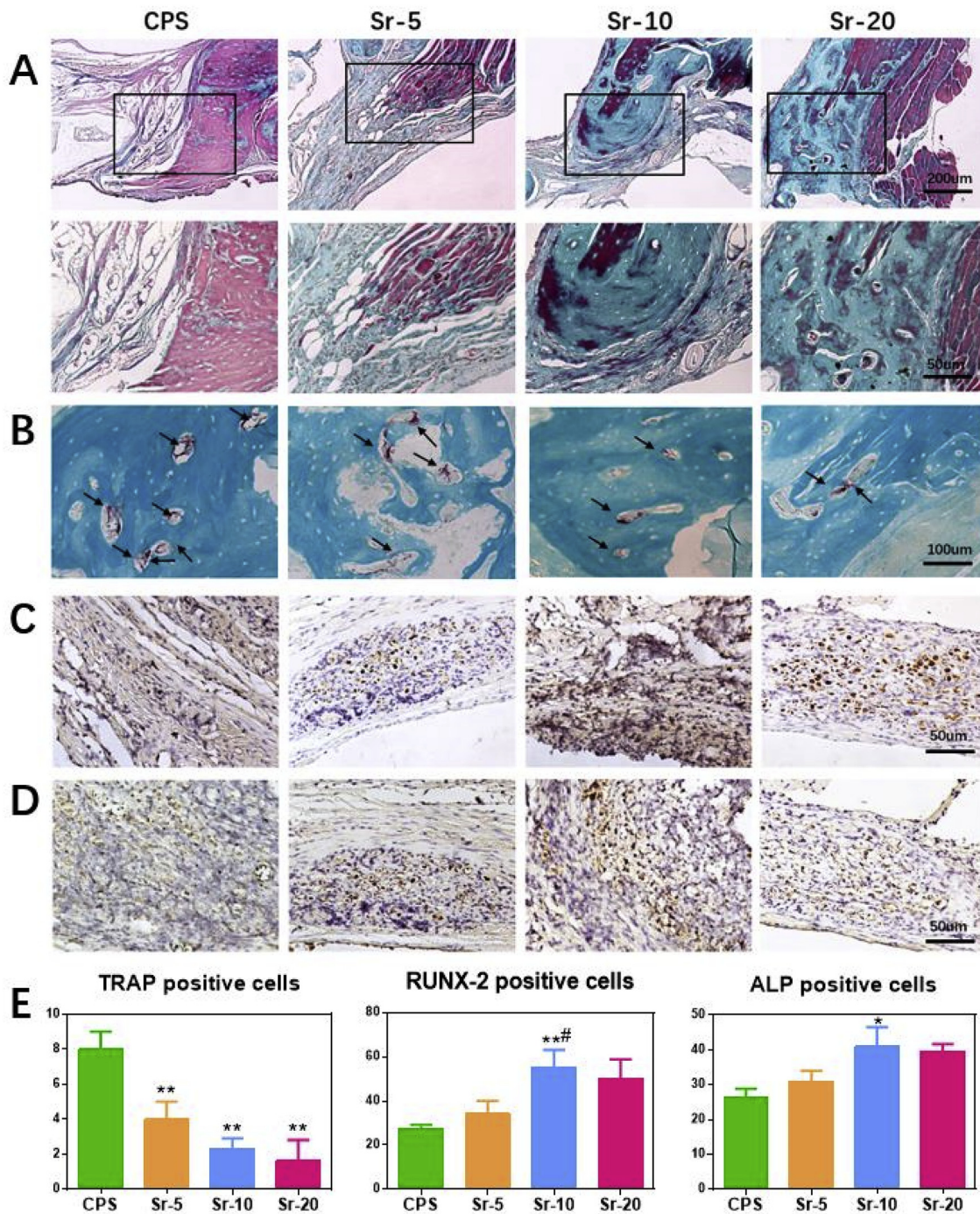


Fig. 9. (A) Masson staining: the region between surrounding bone and scaffold (40x & 100x); (B) TRAP staining: TRAP positive cells (black arrows); (C) IHC staining of RUNX-2; (D) IHC staining of ALP; (E) Quantitative analysis for TRAP staining and IHC staining. * Compared with CPS group; # compared with Sr-5 group.

osteoporosis bone defect. *In vitro*, the effects of Sr-CPS on promoting osteogenesis and inhibiting osteoclastogenesis were dose-dependent with Sr ion concentration. *In vivo*, Sr-10 became the best performing scaffold due to a perfect match of bone formation and scaffold degradation rates. Furthermore, Sr-CPS promoted the osteogenic differentiation of rBMSCs through Wnt/ β -catenin signaling pathway and suppressed RANKL-induced osteoclastogenesis through NF- κ B pathway. All the data indicated that Sr-CPS could be a superior candidate for the reconstruction of osteoporosis-related bone defect.

Author contributions

J. Zeng and J. Guo designed the research. J. Guo and F. Deng carried out the material synthesis and characterization; J. Zeng and Z. Sun conducted the cell experiments and performed the animal surgeries. J. Zeng and J. Guo drafted the manuscript. Y. Xie and C. ning designed and supported the research. All authors read and approved the final manuscript.

5. Declaration of interest statement

The authors declare that they have no known competing financial

interests or personal relationships that could have appeared to influence the work reported in this paper.

CRedit authorship contribution statement

Junkai Zeng: Methodology, Investigation, Writing - original draft. **Jingshu Guo:** Investigation, Writing - original draft. **Zhenyu Sun:** Investigation. **Fanyan Deng:** Validation. **Congqin Ning:** Conceptualization, Resources, Writing - review & editing. **Youzhan Xie:** Supervision, Writing - review & editing.

Declaration of competing interest

The authors declare no conflict of interest.

Acknowledgements

The authors are grateful to the financial support from National Key Research and Development Program of China (Grant No. 2018YFC2002303), National Natural Science Foundation of China (Grant No. 51672304) and International Partnership Program of Chinese Academy of Science (Grant No. GJHZ1760).

Appendix A. Supplementary data

Supplementary data to this article can be found online at <https://doi.org/10.1016/j.bioactmat.2020.03.008>.

References

- [1] T.D. Rachner, S. Khosla, L.C. Hofbauer, Osteoporosis: now and the future, *Lancet* 377 (2011) 1276–1287.
- [2] J.E. Compston, M.R. McClung, W.D. Leslie, Osteoporosis, *Lancet* 393 (2019) 364–376.
- [3] K. Akesson, D. Marsh, P.J. Mitchell, A.R. McLellan, J. Stenmark, D.D. Pierroz, C. Kyer, C. Cooper, Capture the Fracture: a Best Practice Framework and global campaign to break the fragility fracture cycle, *Osteoporos. Int.* 24 (2013) 2135–2152 a journal established as result of cooperation between the European Foundation for Osteoporosis and the National Osteoporosis Foundation of the USA.
- [4] N.E. Lane, Epidemiology, etiology, and diagnosis of osteoporosis, *Am. J. Obstet. Gynecol.* 194 (2006) S3–S11.
- [5] X. Chen, X. Zhi, P. Pan, J. Cui, L. Cao, W. Weng, Q. Zhou, L. Wang, X. Zhai, Q. Zhao, H. Hu, B. Huang, J. Su, Matrine prevents bone loss in ovariectomized mice by inhibiting RANKL-induced osteoclastogenesis, *Faseb. J. : Off. Publ. Feder. Am. Soc. Exp. Biol.* 31 (2017) 4855–4865.
- [6] D.H. Chow, K.S. Leung, L. Qin, A.H. Leung, W.H. Cheung, Low-magnitude high-frequency vibration (LMHFV) enhances bone remodeling in osteoporotic rat femoral fracture healing, *J. Orthop. Res. : Off. Publ. Orthop. Res. Soc.* 29 (2011) 746–752.
- [7] X. Cheng, H.Q. Long, J.H. Xu, Y.L. Huang, F.B. Li, Comparison of unilateral versus bilateral percutaneous kyphoplasty for the treatment of patients with osteoporosis vertebral compression fracture (OVCF): a systematic review and meta-analysis, *Eur. Spine J. : official publication of the European Spine Society, the European Spinal Deformity Society, and the European Section of the Cervical Spine Research Society* 25 (2016) 3439–3449.
- [8] A. Balasubramanian, J. Zhang, L. Chen, D. Wenkert, S.G. Daigle, A. Grauer, J.R. Curtis, Risk of subsequent fracture after prior fracture among older women, *Osteoporos. Int.* 30 (2019) 79–92 a journal established as result of cooperation between the European Foundation for Osteoporosis and the National Osteoporosis Foundation of the USA.
- [9] J. Zhang, W. Liu, V. Schnitzler, F. Tancret, J.M. Bouler, Calcium phosphate cements for bone substitution: chemistry, handling and mechanical properties, *Acta Biomater.* 10 (2014) 1035–1049.
- [10] K.A. Egol, A. Nauth, M. Lee, H.C. Pape, J.T. Watson, J. Borrelli Jr., Bone grafting: sourcing, timing, strategies, and alternatives, *J. Orthop. Trauma* 29 (Suppl 12) (2015) S10–S14.
- [11] W. Duan, C. Ning, T. Tang, Cytocompatibility and osteogenic activity of a novel calcium phosphate silicate bioceramic: Silicocarnotite, *J. Biomed. Mater. Res.* 101 (2013) 1955–1961.
- [12] H. Yuan, H. Fernandes, P. Habibovic, J. de Boer, A.M. Barradas, A. de Ruyter, W.R. Walsh, C.A. van Blitterswijk, J.D. de Bruijn, Osteoinductive ceramics as a synthetic alternative to autologous bone grafting, *Proc. Natl. Acad. Sci. U.S.A.* 107 (2010) 13614–13619.
- [13] M. Motisuke, G. Mestres, C.O. Reno, R.G. Carrodegua, C.A.C. Zavaglia, M.P. Ginebra, Influence of Si substitution on the reactivity of alpha-tricalcium phosphate, *Mater. Sci. Eng. C Mater. Biol. Appl.* 75 (2017) 816–821.
- [14] A.F. Khan, M. Saleem, A. Afzal, A. Ali, A. Khan, A.R. Khan, Bioactive behavior of silicon substituted calcium phosphate based bioceramics for bone regeneration, *Mater. Sci. Eng. C Mater. Biol. Appl.* 35 (2014) 245–252.
- [15] W. Lu, W. Duan, Y. Guo, C. Ning, Mechanical properties and in vitro bioactivity of Ca5(PO4)2SiO4 bioceramic, *J. Biomater. Appl.* 26 (2012) 637–650.
- [16] V. Pavone, G. Testa, S.M.C. Giardina, A. Vescio, D.A. Restivo, G. Sessa, Pharmacological therapy of osteoporosis: a systematic current review of literature, *Front. Pharmacol.* 8 (2017) 803.
- [17] R.M. Hodges, D.N. Mac, R. Nusbaum, R. Stearns, F. Ezmirlan, P. Spain, A.C. Mc, The strontium content of human bones, *J. Biol. Chem.* 185 (1950) 519–524.
- [18] S. Kargozar, M. Montazerian, E. Fiume, F. Baino, Multiple and promising applications of strontium (Sr)-Containing bioactive glasses in bone tissue engineering, *Front. Bioeng. Biotechnol.* 7 (2019) 161.
- [19] G. El-Hajj Fuleihan, Strontium ranelate—a novel therapy for osteoporosis or a permutation of the same? *N. Engl. J. Med.* 350 (2004) 504–506.
- [20] A.J. Sips, W.J. van der Vijgh, R. Barto, J.C. Netelenbos, Intestinal strontium absorption: from bioavailability to validation of a simple test representative for intestinal calcium absorption, *Clin. Chem.* 41 (1995) 1446–1450.
- [21] F. Yang, D. Yang, J. Tu, Q. Zheng, L. Cai, L. Wang, Strontium enhances osteogenic differentiation of mesenchymal stem cells and in vivo bone formation by activating Wnt/catenin signaling, *Stem Cell.* 29 (2011) 981–991.
- [22] S. Zhu, X. Hu, Y. Tao, Z. Ping, L. Wang, J. Shi, X. Wu, W. Zhang, H. Yang, Z. Nie, Y. Xu, Z. Wang, D. Geng, Strontium inhibits titanium particle-induced osteoclast activation and chronic inflammation via suppression of NF-kappaB pathway, *Sci. Rep.* 6 (2016) 36251.
- [23] Z. Chen, E. Cho, J. Lee, S. Lee, T.H. Lee, Inhibitory effects of N-[2-(4-acetyl-1-piperazinyl) phenyl]-2-(2-chlorophenoxy) acetamide on osteoclast differentiation in vitro via the downregulation of TRAF6, *Int. J. Mol. Sci.* 20 (2019).
- [24] J. An, D. Hao, Q. Zhang, B. Chen, R. Zhang, Y. Wang, H. Yang, Natural products for treatment of bone erosive diseases: the effects and mechanisms on inhibiting osteoclastogenesis and bone resorption, *Int. Immunopharm.* 36 (2016) 118–131.
- [25] M.D. O'Donnell, P.L. Candarlioglu, C.A. Miller, E. Gentleman, M.M. Stevens, Materials characterisation and cytotoxic assessment of strontium-substituted bioactive glasses for bone regeneration, *J. Mater. Chem.* vol. 20, (2010) 8934–8941.
- [26] M.D. O'Donnell, Y. Fredholm, A. de Rouffignac, R.G. Hill, Structural analysis of a series of strontium-substituted apatites, *Acta Biomater.* 4 (2008) 1455–1464.
- [27] P. Mcmillan, B.J.B.D.M. Piriou, Raman-spectroscopic studies of silicate and related glass structure—a review, 106 (1983) 57–75.
- [28] S. Minear, P. Leucht, J. Jiang, B. Liu, A. Zeng, C. Fuerer, R. Nusse, J.A. Helms, Wnt proteins promote bone regeneration, *Sci. Transl. Med.* 2 (2010) 29ra30.
- [29] L. Ling, V. Nurcombe, S.M. Cool, Wnt signaling controls the fate of mesenchymal stem cells, *Gene* 433 (2009) 1–7.
- [30] S.L. Holmen, C.R. Zylstra, A. Mukherjee, R.E. Sigler, M.C. Faugere, M.L. Boussein, L. Deng, T.L. Clemens, B.O. Williams, Essential role of beta-catenin in postnatal bone acquisition, *J. Biol. Chem.* 280 (2005) 21162–21168.
- [31] W.J. Boyle, W.S. Simonet, D.L. Lacey, Osteoclast differentiation and activation, *Nature* 423 (2003) 337–342.
- [32] X. Zhi, L. Wang, H. Chen, C. Fang, J. Cui, Y. Hu, L. Cao, W. Weng, Q. Zhou, L. Qin, H. Song, Y. Wang, Y. Wang, H. Jiang, X. Li, S. Wang, X. Chen, J. Su, 1-tetrahydroxypalmitate suppresses osteoclastogenesis in vivo and in vitro via blocking RANK-TRAF6 interactions and inhibiting NF-kappaB and MAPK pathways, *J. Cell Mol. Med.* 24 (2020) 785–798.
- [33] M. Yamaguchi, M.N. Weitzmann, The intact strontium ranelate complex stimulates osteoblastogenesis and suppresses osteoclastogenesis by antagonizing NF-kappaB activation, *Mol. Cell. Biochem.* 359 (2012) 399–407.
- [34] X. Bai, S. Lu, Z. Cao, B. Ni, X. Wang, P. Ning, D. Ma, H. Wei, M. Liu, Dual crosslinked chondroitin sulfate injectable hydrogel formed via continuous Diels-Alder (DA) click chemistry for bone repair, *Carbohydr. Polym.* 166 (2017) 123–130.
- [35] O. Morales, M.K. Samuelsson, U. Lindgren, L.A. Haldosen, Effects of alpha,25-dihydroxyvitamin D3 and growth hormone on apoptosis and proliferation in UMR 106 osteoblast-like cells, *Endocrinology* 145 (2004) 87–94.
- [36] C. Zuo, Y. Huang, R. Bajis, M. Sahih, Y.P. Li, K. Dai, X. Zhang, Osteoblastogenesis regulation signals in bone remodeling, *Osteoporos. Int.* 23 (2012) 1653–1663 a journal established as result of cooperation between the European Foundation for Osteoporosis and the National Osteoporosis Foundation of the USA.
- [37] S.A. Holstein, A patent review of bisphosphonates in treating bone disease, *Expert Opin. Ther. Pat.* 29 (2019) 315–325.
- [38] S.J. Wojda, S.W. Donahue, Parathyroid hormone for bone regeneration, *J. Orthop. Res. : Off. Publ. Orthop. Res. Soc.* 36 (2018) 2586–2594.
- [39] E. Bonnellye, A. Chabadel, F. Salter, P. Jurdic, Dual effect of strontium ranelate: stimulation of osteoblast differentiation and inhibition of osteoclast formation and resorption in vitro, *Bone* 42 (2008) 129–138.
- [40] K. Lin, L. Xia, H. Li, X. Jiang, H. Pan, Y. Xu, W.W. Lu, Z. Zhang, J. Chang, Enhanced osteoporotic bone regeneration by strontium-substituted calcium silicate bioactive ceramics, *Biomaterials* 34 (2013) 10028–10042.
- [41] P. Naruphontjirakul, A.E. Porter, J.R. Jones, In vitro osteogenesis by intracellular uptake of strontium containing bioactive glass nanoparticles, *Acta Biomater.* 66 (2018) 67–80.
- [42] E. Gentleman, Y.C. Fredholm, G. Jell, N. Lotfikhshai, M.D. O'Donnell, R.G. Hill, M.M. Stevens, The effects of strontium-substituted bioactive glasses on osteoblasts and osteoclasts in vitro, *Biomaterials* 31 (2010) 3949–3956.
- [43] P. Yin, F.F. Feng, T. Lei, X.H. Zhong, X.C. Jian, Osteoblastic cell response on bi-phasic fluorhydroxyapatite/strontium-substituted hydroxyapatite coatings, *102* (2014) 621–627.
- [44] D.W. Huttmacher, Scaffolds in tissue engineering bone and cartilage, *Biomaterials* 21 (2000) 2529–2543.
- [45] T.P. Hill, D. Spater, M.M. Taketo, W. Birchmeier, C. Hartmann, Canonical Wnt/beta-catenin signaling prevents osteoblasts from differentiating into chondrocytes, *Dev. Cell* 8 (2005) 727–738.
- [46] Y. Abu-Amer, NF-kappaB signaling and bone resorption, *Osteoporos. Int.* 24 (2013) 2377–2386 a journal established as result of cooperation between the European Foundation for Osteoporosis and the National Osteoporosis Foundation of the USA.